

AIRBORNE REMOTE SENSING TO DETECT PLANT WATER STRESS IN FULL CANOPY COTTON

W. R. DeTar, J. V. Penner, H. A. Funk

ABSTRACT. *The potential for monitoring plant water stress in full-canopy cotton using airborne remote sensing was examined in this study. Remote sensing data, using hyperspectral (HSI), multispectral (MSI), and thermal infrared (TIR) sensors, were collected over two seasons on two varieties of Acala cotton and two experimental fields, with a total of nine flights, all with 100% canopy cover. The spatial resolution of the remote sensing data used in the study was near 1.0 m. The TIR camera was used to detect the elevated canopy temperature that occurs when the plants are water stressed. The degree of stress, as measured by the rise in canopy temperature above an unstressed baseline, was closely related to several new vegetation indices that use spectral bands in the range of 429 to 1010 nm. Both linear and nonlinear multiple regression were used to find the wavelengths that produced the highest coefficient of determination (r^2) and lowest root mean square error (RMSE) for one-, two-, three-, and four-parameter HSI models. The MSI-based vegetation indices had significant correlations to plant water stress, but the r^2 values were lower than those with the HSI data. The best two-parameter HSI models included one band each from the near-infrared (NIR; 850 nm) and visible (686 nm) ranges. The best three-parameter model used the bands centered at 686, 811, and 860 nm. A weighted normalized difference vegetation index (NDVI) was found to correlate well to water stress with $r^2 = 0.883$. The average reflectance over the range of 923 nm to 1010 nm was found to be an indicator of differences in the canopy temperature. The main finding was that the plant water stress in Acala cotton at full canopy can be detected with airborne remote sensing, and this should greatly enhance the ability to properly schedule irrigations.*

Keywords. *Cotton, Hyperspectral imagery, Irrigation, Multispectral imagery, Precision farming, Spectral response patterns, Vegetation indices.*

Remote sensing can provide the spatial distribution of varying crop growth and conditions that are required for precision farming (Maas, 1998; Moran et al., 1997; Dawson, 1997). Many vegetation indices have been used to empirically relate remotely sensed data to crop properties (Thenkabail et al., 2000; Thorp et al., 2004). Goel et al. (2003) found that various functions of the normalized difference vegetation index (NDVI) correlated better and showed more consistency than multiple regression models developed from airborne hyperspectral data for nine different properties of a corn crop.

Plant water stress is a major factor affecting crop yield. Irrigation to avoid or relieve this stress must be done judiciously, not only to avoid environmental problems such as groundwater pollution and runoff, but also to keep the cost down on a limited and expensive resource. The temperature of the plant canopy has been used for sensing plant water stress ever since the development of the infrared thermometer made this measurement possible without physically touching the plant (Ehrler et al., 1978). A study by Moran et

al. (1989) showed that water stress on alfalfa affected the canopy architecture and reduced the spectral reflectance in both the near-infrared (NIR) and red regions. Jackson et al. (1983) used several ratios and linear combinations of bands, and concluded that water stress on wheat could not be detected until there was a stress-induced retardation in growth. Peñuelas et al. (1996) showed a linear relationship between relative water content (RWC) and the water index (WI), which is the reflectance ratio R_{900}/R_{970} , for wheat at full canopy.

For cotton, Bowman (1989) found that the relative reflectance at 810, 1665, and 2210 nm wavelengths increased as RWC decreased. Jackson et al. (1981) showed that the degree of plant water stress is directly proportional to the rise in the canopy temperature above an unstressed baseline temperature. This rise in canopy temperature was also the basis for the work done by Wanjura and Upchurch (2000) on cotton and corn. The baseline canopy temperature is the temperature of the canopy for healthy, well-watered plants. Because of an evaporative cooling effect, it is several degrees below air temperature, depending on the vapor pressure deficit (VPD) of the air above it. Plant et al. (2000) were able to relate the onset of water stress in cotton to NDVI. Maas et al. (1999) showed the effects of developing moisture stress, as indicated by a rise in canopy temperature, using airborne thermal infrared (TIR) data from daily flights over drip-irrigated cotton plots suddenly deprived of water. Temperatures rose by as much as 10°C above those in unstressed plots.

Because of the natural variability of soil in any large field, determining the proper time to irrigate a large field of cotton is difficult. In those parts of the field that are not stressed,

Submitted for review in October 2005 as manuscript number SW 6132; approved for publication by the Soil & Water Division of ASABE in May 2006.

The authors are **William R. DeTar**, ASABE Member Engineer, Research Agricultural Engineer, **John V. Penner**, Engineering Technician, and **Howard A. Funk**, Research Technician, USDA-ARS Western Integrated Cropping Systems Research Unit, Shafter, California. **Corresponding author:** William R. DeTar, USDA-ARS, 17053 N. Shafter Ave., Shafter, CA 93263; phone: 661-746-8011; fax: 661-746-1619; e-mail: wrdetar@pw.ars.usda.gov.

irrigating too early can lead to rank growth and reduced yield. In other parts of the field, the soil may have a lower water holding capacity, or rooting depth may be limited, and irrigating too late can cause excessive stress, again reducing yield. Timing the irrigation based on what the irrigator can see from the edge of the field can be misleading. It would be helpful in planning and managing the irrigation system to know the degree of plant water stress in every part of the field. Thus, the aim of this study was to use airborne multispectral and hyperspectral data to produce prediction models that would provide detailed maps of plant water stress in cotton.

MATERIALS AND METHODS

EXPERIMENTAL FIELDS

The site for this study was the Shafter Research and Extension Center of the University of California, which is located near the southern end of the San Joaquin Valley, at 35° 31' N, 119° 17' W, and 109 m above sea level. Annual average precipitation is 167 mm, of which only 8 mm occurs during the growing season. All the soils on the station are mapped as a Wasco sandy loam (coarse-loamy, mixed, non-acid, thermic Typic Torriothents). In 2001, Acala NemX cotton was grown in field 42, which is a 2.6 ha field, 85 m wide by 302 m long. Plant row spacing was 0.76 m, and the rows ran in the east-west direction. The field had been previously laser-leveled to zero side slope and a 0.5% slope down from east to west. A subsurface drip irrigation system was used, with drip lines buried 0.26 m below grade, one in every plant row and running the full length of the field. Water was applied on a daily basis.

The field was divided into four narrow strips, each 21.3 m wide. Each of these strip plots was on a separate irrigation circuit, and they were labeled 42A, 42B, 42C, and 42D from south to north (fig. 1). Plots 42B and 42D were irrigated normally, applying the average ET required (see DeTar, 2004) based on a system efficiency of 90%. In order to simulate a furrow- or sprinkler-irrigated heavier soil where an irrigation would be required about once every four weeks, plots 42A and 42C were deficit-irrigated by about 25% starting 25 June 2001, applying an average of 1.9 mm/d less than the depth normally required. The average moisture available in the root zone was about 127 mm at field capacity.

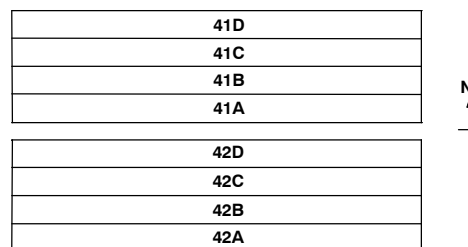


Figure 1. Plot plan.

Allen et al. (1998) gave the threshold point for start of water stress at 56% depletion when the normal crop ET is 7.1 mm/d. So the plan was to reach this point in $127 \times 0.56 / 1.9 = 37$ days, which would be 1 August, well past the date at which full canopy should have been reached. Partial canopy was being avoided because of the influence that exposed bare soil between the plant rows has on the scene temperatures.

In 2002, an adjacent field (field 41) was planted to Acala PhytoGen-72 cotton. It had the same dimensions, layout, and irrigation system as in field 42. But in this case plots, 41B and 41D were deficit-irrigated starting on 27 June 2002, and plots 41A and 41C were irrigated normally.

EQUIPMENT AND GROUND TRUTHING FOR FLIGHTS

Over the two years, data acquisition flights were made between 19 July and 28 August each year, a period with full canopy cover. The flights in 2001 were made almost weekly; however, in 2002, there were fewer flights because of limited funding. The light airplane (Cessna 206/210), pilot, camera operator, and pre-processing were all provided by Opto-Knowledge Systems, Inc., (OKSI) of Torrance, California. OKSI also provided a hyperspectral (HSI) camera, called the Airborne Visible/Near-Infrared (AVNIR) system, which had a spatial resolution of 0.8 m from an altitude of 1500 m, with 60 bands of reflectance data in the range of 429 to 1010 nm and a spectral resolution of 10 nm. Because of the numerous references that must be made to different bands in the data processing and presentation, band numbers were often used in this study instead of wavelengths. The band numbers and their associated wavelengths are given in table 1.

Also included from all flights were data from a set of cameras provided by the USDA-ARS at Shafter, called the Shafter Airborne Multispectral (MSI) Remote Sensing

Table 1. Wavelengths and corresponding band numbers used in the hyperspectral analysis.

Band		Band		Band		Band	
Center (nm)	No.						
1005.1	B1	859.86	B16	714.61	B31	569.36	B46
995.43	B2	850.18	B17	704.93	B32	559.68	B47
985.75	B3	840.49	B18	695.24	B33	549.99	B48
976.06	B4	830.81	B19	685.56	B34	540.31	B49
966.38	B5	821.13	B20	675.88	B35	530.63	B50
956.70	B6	811.44	B21	666.19	B36	520.94	B51
947.01	B7	801.76	B22	656.51	B37	511.26	B52
937.33	B8	792.08	B23	646.83	B38	501.58	B53
927.65	B9	782.39	B24	637.14	B39	491.89	B54
917.96	B10	772.71	B25	627.46	B40	482.21	B55
908.28	B11	763.03	B26	617.78	B41	472.53	B56
898.60	B12	753.34	B27	608.09	B42	462.84	B57
888.91	B13	743.66	B28	598.41	B43	453.16	B58
879.23	B14	733.98	B29	588.73	B44	443.48	B59
869.55	B15	724.29	B30	579.04	B45	433.79	B60

System (SAMRSS) developed by Maas et al. (1999). This package included three Dalsa digital cameras (Dalsa, Inc., Waterloo, Ontario, Canada) each with a different filter, one for the green range of 545 nm to 555 nm, one for the red range of 675 nm to 685 nm, and one near-infrared (NIR) camera for the range 830 nm to 870 nm, all with a spatial resolution of 1 m. Included in the package was a thermal infrared (TIR) camera (Indigo Merlin thermal imager from Indigo Systems, Santa Barbara, Cal.) with a range of 8,000 nm to 14,000 nm and a spatial resolution of 2.4 m, and in addition there was a video camera.

On flight days, three 8 × 8 m fabric calibration panels (Tracor Aerospace, Inc., Austin, Texas) were spread out on the unpaved road at the east end of field 41. As near flight time as possible, ground truthing was done with hand-held infrared thermometers (Oakton InfraPro 3, Lesman Instrument Co., Bensenville, Ill.), obtaining temperatures of unpaved roads, fallowed fields, smooth bare soil walkways, stressed and unstressed canopies, calibration panels, a pond, unplanted but furrowed and cultivated soil at the east end of field 42, and nearby alfalfa fields. Air temperature and humidity (dry bulb and wet bulb) were measured above the canopy in the field and also in areas around the field with a battery-aspirated psychrometer (Psychron model 566, Belfort Instrument Co., Baltimore, Md.). Spectral radiometer readings of the calibration panels were also taken using a model LI-1800 (Li-Cor, Inc., Lincoln, Neb.). All these, along with data from the Research Center's weather station, were sent to OKSI within 3 h after the flight for pre-processing. Normal turn around time for the processing was about 24 h.

DATA ANALYSIS

Using ENVI, an image processing software (Research Systems, Inc., Boulder, Colo.), images for both fields 41 and 42 were extracted from larger images acquired during the flights and exported as ASCII files for further processing. Excel was then used to convert these files to a format useable by CoPlot v3.0 (CoHort Software, Monterey, Cal.) and by ArcView GIS v3.3 (ESRI, Redlands, Cal.). For each flight date, there were three categories of data: HSI, MSI, and TIR. The initial procedure in ArcView is essentially the same for all three categories. In 2001 for example, strip plots 42B and 42C were each subdivided into ten grids measuring 21.3 × 30.2 m. Each of these grids was first selected, leaving a one-pixel margin around the edge to act as a buffer; then, by opening a theme table and selecting a field heading (band), it was possible to get statistics for that grid area. For the TIR data, there were only three columns of data (longitude, latitude, and temperature), and the only statistic recorded was the average temperature for that grid area. For the MSI data, there were five columns of data: longitude, latitude, and the reflectance for the green, red, and NIR bands. The averages for each reflectance band were recorded for that grid area. The same could have been done for the HSI data, but it would have been tedious because there are 60 bands. So the HSI data for each grid area were exported to a separate Excel file, where the averages for each band were easily calculated. The averages from each grid area were accumulated in a separate file, one grid area to each row. The average spectral response patterns for stressed versus unstressed treatments for each flight were developed from this file. This grid-area file of 20 rows and 60 columns became the primary source for regression analysis for each flight, when temperature data

were inserted into column 61. For validation purposes, the entire procedure was repeated using the A and D plots of fields 41 and 42.

UNSTRESSED BASELINE CANOPY TEMPERATURES

The VPD depends on the temperature and humidity of the air above the crop canopy. For cotton under the arid conditions of the Central Valley of California, the VPD ranges typically from 2 to 4 kPa, and the corresponding difference between well-watered canopy and air temperature is 3°C to 6.5°C. This relationship was determined for the conditions locally in 2001 with the same hand-held IR thermometer and psychrometer used during the ground truthing for flights. The results, shown in figure 2, agree closely with those of Howell et al. (1984), Pinter and Reginato (1982), and Idso et al. (1982). The regression equation is:

$$T_b - T_a = 0.597 - 1.779*P \quad (1)$$

where P is the vapor pressure deficit of air (kPa), T_b is the unstressed baseline canopy temperature (°C), and T_a is the air temperature (°C). The RMSE was 0.534°C, and the maximum residual was 1.10°C. Rearranging equation 1, the baseline temperature is:

$$T_b = T_a + 0.597 - 1.779*P \quad (2)$$

There is an upper limit to canopy temperatures, where the leaves have completely stopped transpiring; it is independent of the VPD, and it is generally thought to be 4°C to 6°C above air temperature. So under some extreme conditions, the rise in canopy temperature above the unstressed baseline could be as much as 12°C. It is this rise in canopy temperature above the lower baseline that we now use to correlate stress to the MSI and HSI data.

The VPD above the canopy was measured at several places in the cotton field, during, before, and after each flight. From this, a theoretical unstressed baseline temperature was calculated using equation 1. There is a slight problem with the normal scatter around the baseline. The well-watered canopy temperature can easily be 1°C above, or below this baseline equation, depending on atmospheric conditions. It

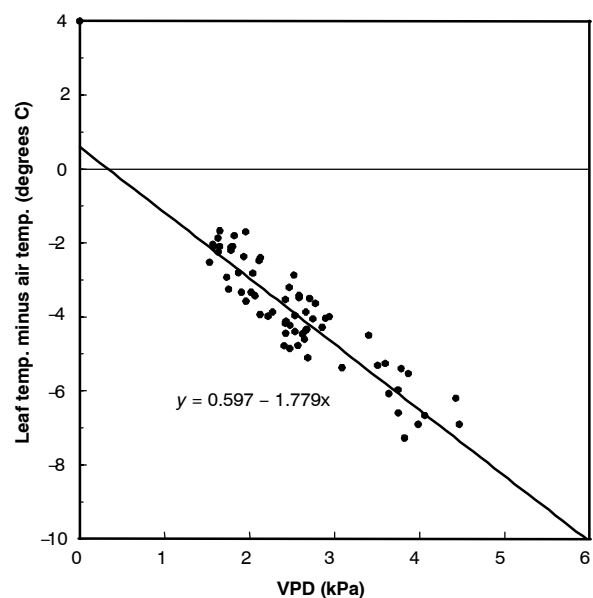


Figure 2. Unstressed baseline canopy temperature for Acala cotton.

is an excellent guide, but it is better to use the lowest temperature seen in the TIR image as a reference, if the cotton plants there are known to be in good soil, healthy, and well watered with 100% canopy. This latter condition was available for almost all the flights, and when it was not, the theoretical baseline was used. When there is some doubt about the coolest place on the TIR image being stress free, it is important to have the second source for verification. In general, baseline temperatures from the two sources agreed quite well.

As stated above, the plant water stress is directly proportional to the rise of canopy temperature above the unstressed baseline. This rise can be expressed as:

$$T_r = T_c - T_b \quad (3)$$

where T_c is the canopy temperature at any degree of stress as measured by the TIR camera, and T_r is the rise in canopy temperature above the unstressed baseline, a measure of plant water stress. The value for T_r for each grid area was calculated by subtracting the T_b from each of the average grid values of TIR. These values of T_r were then inserted into column 61 of the HSI data, and also into column 4 of the MSI data.

MULTIPLE LINEAR REGRESSION

The combination of bands in the HSI grid-area files that best correlated to the plant water stress were found by first importing the files into CoPlot, one data set for each of nine flights. Initially, each flight was analyzed separately. The temperature rise (T_r) was considered the dependent variable, and the various band reflectances were the independent variables. There is a procedure available in CoPlot in which, after a choice is made of the number of bands to include in each multiple regression, the program looks at every possible combination. The number of regressions required for pairs of bands out of 60 available is $60 \cdot 59 / (1 \cdot 2) = 1770$. To find the best 3-band combinations requires $60 \cdot 59 \cdot 58 / (1 \cdot 2 \cdot 3) = 34,220$ regressions, and 4-band combinations require 487,635 regressions. CoPlot uses matrix manipulation of simultaneous equations with an accuracy of ten significant figures and tests for collinearity. The program automatically ranks and stores the results of the 100 best combinations (models). The MSI data were processed the same way, but this required far fewer regressions because there were only three bands available to analyze.

The models were evaluated by comparing the observed and predicted values. The root mean square error (RMSE), the average relative percent error (ARPE) from Jakeman et al. (1990), the coefficient of efficiency (EFF) from Nash and Sutcliffe (1970), and the coefficient of determination (r^2) were calculated for both the model calibration and the validation data:

$$RMSE = \sqrt{\frac{\sum_{i=1}^{i=n} (P_i - O_i)^2}{n}} \quad (4)$$

$$ARPE = \frac{\sum_{i=1}^{i=n} (P_i - O_i)}{\sum_{i=1}^{i=n} O_i} \quad (5)$$

$$EFF = \frac{\sum_{i=1}^{i=n} (O_i - \bar{O})^2 - \sum_{i=1}^{i=n} (P_i - O_i)^2}{\sum_{i=1}^{i=n} (O_i - \bar{O})^2} \quad (6)$$

$$r^2 = \left[\frac{\sum_{i=1}^{i=n} (O_i - \bar{O})(P_i - \bar{P})}{\left(\sqrt{\sum_{i=1}^{i=n} (O_i - \bar{O})^2} \right) \left(\sqrt{\sum_{i=1}^{i=n} (P_i - \bar{P})^2} \right)} \right]^2 \quad (7)$$

where

O_i = individual observed value

P_i = individual predicted value

\bar{O} = mean observed value

\bar{P} = mean predicted value

n = number of paired values.

The RMSE is an indicator of the scatter around the regression line, while the ARPE expresses the error, and the sign of the error indicates whether the model over- or underestimated the values. The EFF term evaluates the error relative to natural variation in the observed values, and varies from $-\infty$ to 1, with EFF values greater than zero indicating that the model is a good predictor. The r^2 ranges from 0 to 1, with the higher values indicating better agreement between predicted and observed values, and depends in part on the range of values included, the slope, and the RMSE. The r^2 evaluates only linear relationships between variables, whereas the EFF is sensitive to differences in the means and variances and is a better measure to evaluate model simulations (Lagates and McCabe, 1999).

RESULTS AND DISCUSSION

SPECTRAL RESPONSE PATTERNS

Some examples of how plant water stress affect the spectral response curves are shown in figure 3. In each case, the average band reflectance for the entire stressed plot is plotted along with that for the entire unstressed plot. The difference between the two is also plotted. In the case of figure 3a, which shows the spectral response curve for the flight of 25 July 2001, the stressed plot is 42C (field 42, plot C), and the unstressed plot is 42B (field 42, plot B). Figures 3a and 3c are for flights during relatively low-stress periods, and figures 3b and 3d are for high-stress periods. In comparing one flight to another, there is a considerable difference in the peaks, valleys, slopes, and general magnitude in the NIR region. Most of these irregularities have nothing to do with the stress treatments. Both the stressed and unstressed curves in each flight have nearly the same shape, and the result is an almost constant difference over a large range of wavelengths. The most notable effect of stress is the increased difference in the response curves for wavelengths greater than 760 nm, in the NIR region, with the stressed treatment having the lower reflectance values.

The difference between the average temperature of the entire stressed plot (T_s) and the entire unstressed plot (T_o) was considered to be a measure of stress. This is plotted against time in figure 4a for 2001 and in figure 5a for 2002. One

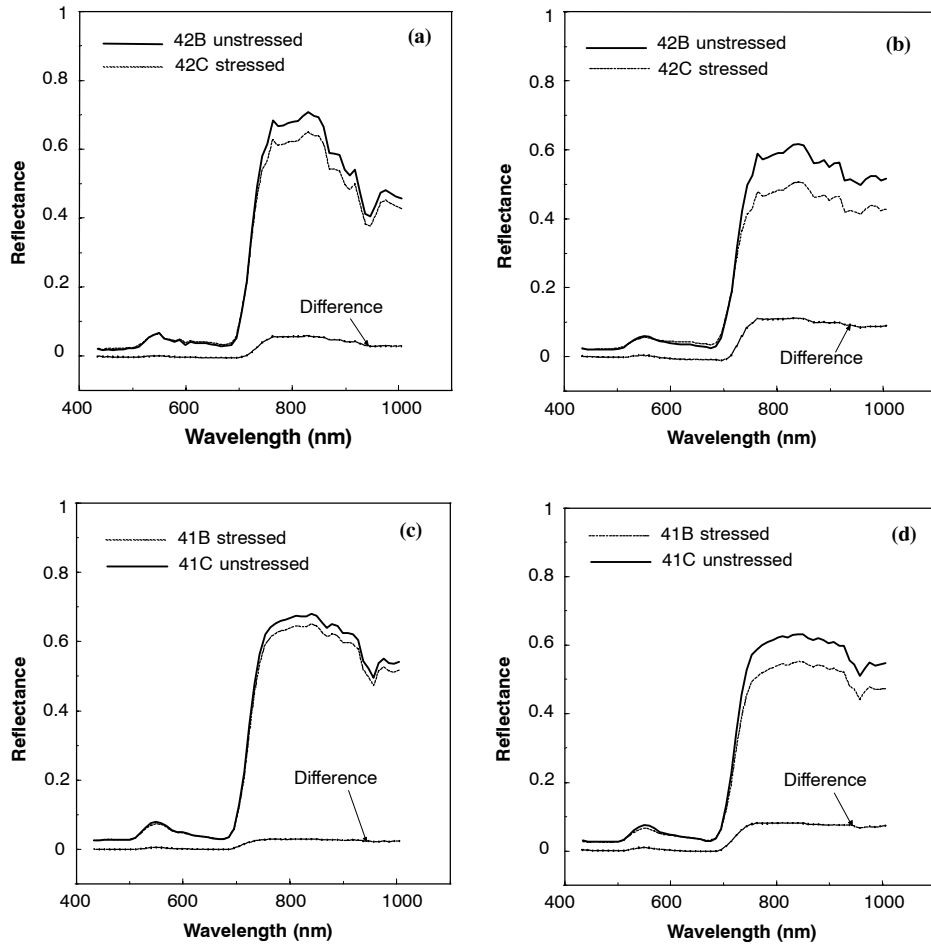


Figure 3. Spectral response patterns for B and C plots: (a) low stress difference, field 42, 25 July 2001; (b) high stress difference, field 42, 16 August 2001; (c) low stress difference, field 41, 31 July 2002; and (d) high stress difference, field 41, 14 August 2002.

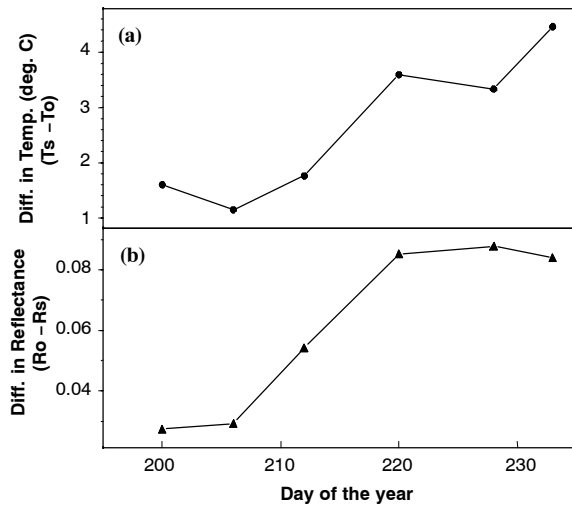


Figure 4. (a) Differences in the average plot temperature for stressed vs. unstressed treatments in 2001, and (b) differences in average broadband NIR (B1 to B9) reflectance over time.

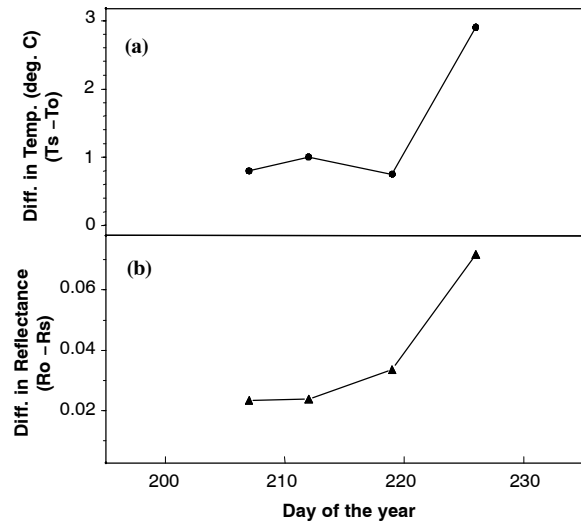


Figure 5. (a) Differences in average plot temperature for stressed vs. unstressed treatments for 2002, and (b) differences in average broadband NIR (B1 to B9) reflectance over time.

typical characteristic of plant water stress is that it tends to happen without much warning or lead-time. This is shown clearly in figure 5a, where little stress is shown until after DOY 220 (8 August), when the average temperature differ-

ence rises by over 2°C in 7 days. By plotting average differences in a range of NIR reflectance values over time on the same graph with the temperature differences (figs. 4b and 5b), one can easily see that they behave in a similar manner.

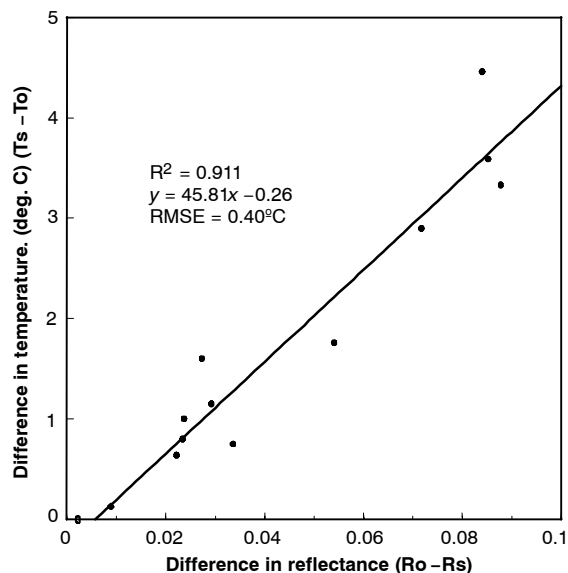


Figure 6. Difference in average plot temperature for stressed vs. unstressed treatments as a function of the broadband NIR (B1 to B9) reflectance.

The range of NIR reflectance values used was the average of bands B1 through B9 (923 nm to 1010 nm). R_o denotes the average NIR reflectance for the unstressed plot, and R_s denotes the same for the stressed plot.

To determine the actual relationship, the difference in the plot temperatures is plotted against $R_o - R_s$ in figure 6. The r^2 of 0.911 is quite good, with a root mean square error (RMSE) of 0.40°C , which is less than the normal variability around the baseline for uniform, unstressed plants. This RMSE is also only 1.3% of the average canopy temperature for the four flights, which was 29.8°C . The efficiency of the regression is 0.968. The result is relative, not absolute, i.e., the difference in the average B1-B9 reflectance value for two different parts of a field is correlated to the difference in the canopy temperature. We can predict that one part of a field has a much higher temperature than another part, but we cannot predict the actual temperatures with this procedure.

MULTIPLE REGRESSION

Using multiple linear regression, the rise in the average canopy temperature above the unstressed baseline for each individual grid area (T_r) was found to be correlated to several

combinations of bands. The models with the highest r^2 for one band, two bands, and three bands are given in table 2 for each of the nine individual flights. Some of the single-band models had low, but still significant, r^2 values. The r^2 values for 2-band models were generally very good, all greater than 0.86. Increasing the number of parameters (bands) in the regression analysis generally increased the r^2 value, but in several cases the increase was not significant. In looking at the 100 best models for each individual flight, it was found to be nearly impossible to find a set of bands that worked consistently well on all of the flights. Occasionally, the same set of bands, from somewhere in the top 100 r^2 values of each flight, was found to work well in two or three flights, but even then, the equations were dissimilar, e.g., with different signs on the coefficients. This problem with consistency was noted by Goel et al. (2003). The problem was also addressed in a comprehensive study by Thenkabail et al. (2000), using stepwise linear regression analysis. One way to find a consistent model for all the flights was to merge all the data into one large file before regressing. So data sets were combined for all six of the 2001 flights, and then another set of nine flights was set up by adding in the three flights from 2002.

The models with the highest r^2 in the combined flights are given in table 3. Merging the database from the 9-flight data caused more scatter and generally reduced the r^2 . This was probably due to the broader range of field and atmospheric conditions encountered. The ten best 2-band models for the 6-flight and 9-flight combinations are given in table 4, and the best 3-band models are given in table 5. It is important to notice here that there are a lot of different combinations that work well, all with $r^2 > 0.9$, and it is obvious that there is not just one, unique solution. Band B34 (686 nm) appears most frequently in the 40 models listed in tables 4 and 5.

Figure 7 shows how well the data from one of the 2-band models fit the linear regression line (the dashed line) for the 6-flight combination. The x-axis for this plot was developed by starting with the linear multiple regression equation:

$$T_r = a - b \cdot R_{24} + c \cdot R_{52} \quad (8)$$

where R_{24} and R_{52} are the reflectances for bands B24 and B52, respectively, and in this case $a = 9.08$, $b = 24.54$, and $c = 263.3$, with $r^2 = 0.948$ and $\text{RMSE} = 0.638^\circ\text{C}$. Equation 4 can also be written as:

$$T_r = a - b \cdot (R_{24} - m \cdot R_{52}) \quad (9)$$

Table 2. Bands with highest r^2 for each individual flight using multiple linear regression on hyperspectral data.

Flight	Year	Date	1-Parameter		2-Parameter		3-Parameter	
			Band	r^2	Bands	r^2	Bands	r^2
1	2001	July 19	B36	0.749	B38, B52	0.924	B38, B52, B55	0.954
2	2001	July 25	B38	0.836	B34, B35	0.868	B32, B52, B55	0.925
3	2001	8 August	B5	0.961	B5, B34	0.980	B14, B22, B35	0.988
4	2001	6 August	B38	0.936	B30, B42	0.985	B30, B46, B48	0.988
5	2001	21 August	B8	0.914	B29, B55	0.978	B29, B54, B55	0.986
6	2001	28 August	B8	0.917	B14, B26	0.959	B14, B24, B26	0.984
7	2002	31 July	B5	0.843	B10, B11	0.870	B7, B53, B55	0.923
8	2002	7 August	B53	0.664	B8, B15	0.878	B8, B15, B17	0.942
9	2002	14 August	B6	0.941	B7, B9	0.965	B23, B28, B48	0.981

Table 3. Bands with the highest r² for combined flights using multiple linear regression on hyperspectral data.

6 Flights		9 Flights	
Bands	r ²	Bands	r ²
B25	0.479	B25	0.547
B14, B52	0.951	B17, B34	0.931
B14, B34, B57	0.962	B16, B21, B34	0.940
B18, B33, B34, B39	0.966	B1, B11, B28, B39	0.949

Table 4. Bands with the ten highest r² for combined flights using 2-parameter multiple linear regression on hyperspectral data.

6 Flights		9 Flights	
Bands	r ²	Bands	r ²
B14, B52	0.951	B17, B34	0.931
B15, B34	0.949	B16, B34	0.930
B14, B56	0.949	B18, B34	0.930
B24, B52	0.948	B19, B34	0.927
B18, B52	0.948	B22, B34	0.923
B28, B52	0.947	B23, B34	0.922
B14, B54	0.947	B24, B34	0.920
B16, B52	0.947	B21, B34	0.920
B14, B51	0.947	B29, B34	0.919
B14, B58	0.946	B26, B34	0.919

Table 5. Bands with the ten highest r² for combined flights using 3-parameter multiple linear regression on hyperspectral data.

6 Flights		9 Flights	
Bands	r ²	Bands	r ²
B14, B34, B57	0.962	B16, B21, B34	0.940
B14, B34, B56	0.962	B17, B25, B34	0.939
B14, B34, B58	0.961	B1, B26, B34	0.938
B28, B45, B52	0.961	B17, B23, B34	0.938
B28, B46, B52	0.961	B3, B26, B34	0.938
B28, B47, B52	0.960	B17, B24, B34	0.937
B14, B36, B60	0.960	B2, B26, B34	0.937
B14, B38, B60	0.960	B3, B19, B34	0.937
B15, B34, B56	0.959	B6, B17, B34	0.937
B14, B37, B60	0.959	B3, B17, B34	0.937

where $m = c/b$, and the expression in the parentheses is a type of vegetation index, which can be expressed as:

$$I_{24-52} = R24 - m \cdot R52 \quad (10)$$

with $m = 10.729$. Substituting equation 6 into equation 5 produces:

$$T_r = a - b \cdot I_{24-52} \quad (11)$$

a simple linear equation, plotted as the dashed line in figure 7.

Table 6. Vegetation indices and nonlinear equations for some of the 2-parameter models with high r², using the equation of the form $T_r = (c_1 - c_2 \cdot I + c_3 \cdot I^2) \cdot e^{(I/c_4)}$ on hyperspectral data.

Flight Combinations	Vegetation Index (I)	c ₁	c ₂	c ₃	c ₄	r ²	RMSE (°C)
6 Flights	R24 - 10.729*R52	9.48	42.00	46.61	0.72	0.962	0.55
	R28 - 9.940*R52	9.20	49.97	69.07	0.56	0.961	0.55
	R18 - 11.121*R52	9.95	42.77	46.14	0.67	0.961	0.55
	R14 - 9.284*R52	10.73	51.39	61.48	0.52	0.959	0.56
	R14 - 10.261*R56	12.22	53.26	58.13	0.52	0.959	0.57
9 Flights	R17 - 4.450*R34	12.21	38.49	30.34	0.60	0.939	0.63
	R14 - 10.255*R56	12.97	52.86	53.97	1.00	0.937	0.64
	R15 - 9.167*R58	14.77	58.44	58.04	1.10	0.937	0.64
	R27 - 9.391*R52	9.94	44.18	49.25	1.40	0.934	0.66
	R24 - 9.800*R52	10.47	42.28	42.84	1.60	0.934	0.66

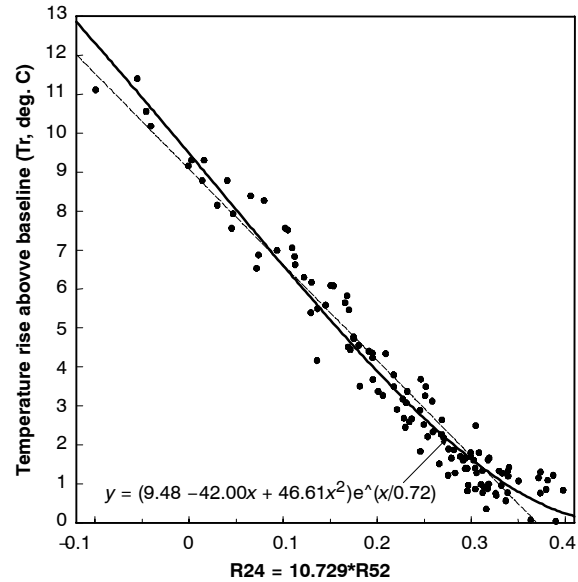


Figure 7. Rise in canopy temperature as a function of a 2-parameter HSI vegetation index for all data from 6 flights in 2001. For the non-linear function: r² = 0.962 and RMSE = 0.55° C.

Equations 3 and 11 were used to predict the canopy temperatures in field 42 for a flight on 31 July 2001, when the TIR camera had failed. The resulting average temperature for some of the unstressed grid areas was considerably below the baseline. This situation was caused by the fact that by using the linear expression in equation 11, the T_r values go negative at the higher, well-watered, values for I_{24-52} . To avoid this problem, a curvilinear function was established for the data in figure 7, so that T_r approaches zero at large values of I_{24-52} . This function is the solid line in figure 7 and is of the form:

$$T_r = (c_1 + c_2 \cdot I + c_3 \cdot I^2) \cdot e^{(I/c_4)} \quad (12)$$

The coefficients c_1 , c_2 , and c_3 were evaluated by a nonlinear multiple regression program in CoPlot, after various values for c_4 were selected manually to force the minimum value of the function to zero. For the data in figure 7, these coefficients were 9.48, -42.00, 46.61, and 0.72, respectively. Several different vegetation indices were fitted this way for some of the better flight combinations, and the results are shown in tables 6 and 7. In the 22 models shown, band B52 appears most often (eight times). Bands B16 and B34 both appear seven times. It should be noted that the r^2 for the non-linear functions was always higher than for

Table 7. Vegetation indices and nonlinear equations for some of the 3- and 4-parameter models with high r^2 , using the equation of the form $T_r = (c_1 - c_2 * I + c_3 * I^2) * e^{(I/c_4)}$ on hyperspectral data.

Flight Combinations	Vegetation Index (I)	c_1	c_2	c_3	c_4	r^2	RMSE (°C)
6 Flights	$-R12 + 2.226 * R14 - 11.20 * R52$	11.05	40.05	36.42	0.65	0.968	0.50
	$R28 + 4.081 * R45 - 15.15 * R52$	10.22	51.97	66.01	0.45	0.968	0.50
	$R14 - 2.162 * R34 - 4.465 * R57$	12.57	48.46	46.65	0.48	0.968	0.50
	$-R6 + 4.119 * R14 - 28.62 * R52$	11.29	15.73	5.49	1.70	0.968	0.50
	$R14 - 3.656 * R36 - 3.868 * R60$	11.53	48.50	51.04	0.42	0.966	0.51
6 Flights	$R18 + 7.57 * R33 - 5.20 * R34 - 9.86 * R39$	12.34	37.20	28.08	0.55	0.971	0.47
9 Flights	$R16 - 0.639 * R21 - 1.318 * R34$	14.07	127.8	290.2	0.20	0.948	0.58
	$R17 - 0.612 * R25 - 1.804 * R34$	13.07	99.16	188.3	0.23	0.947	0.59
	$R16 - 3.269 * R34 - 2.773 * R54$	12.44	41.96	35.39	0.65	0.944	0.60
	$R22 - 0.615 * R27 - 1.872 * R34$	12.58	89.50	159.3	0.29	0.944	0.61
	$R6 + 2.932 * R17 - 17.27 * R34$	12.00	10.29	2.20	2.20	0.943	0.61
9 Flights	$R1 - 0.88 * R11 + 0.61 * R28 - 4.66 * R39$	7.30	61.22	128.4	0.29	0.955	0.54

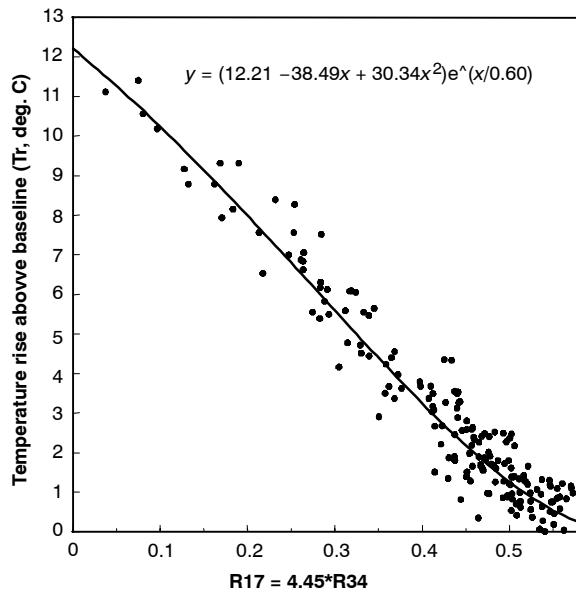


Figure 8. Rise in canopy temperature as a function of a 2-parameter HSI vegetation index for all data from 2001 and 2002 (9 flights): $r^2 = 0.939$ and RMSE = 0.63°C .

the linear functions. In the case of the models in figure 7, going from linear to non-linear increased r^2 from 0.948 to 0.962

and reduced the RMSE from 0.64°C to 0.55°C . An example of one of the better-fitting nonlinear regression equations for the 2-band, 9-flight combination is shown in figure 8. For figure 8, the improvement in r^2 was from 0.931 to 0.939, and the RMSE dropped from 0.67°C to 0.63°C . These results indicate that in some cases there is a slight curvature in the basic data relating temperature rise to the new vegetation indices.

MULTISPECTRAL ANALYSIS

The MSI models shown in tables 8 and 9 have relatively low r^2 values, and a lot of scatter is shown in figures 9 and 10, so it appears that the bands that were used in MSI were not quite close enough to the proper wavelength for the best detection of plant water stress. The 3-parameter, nonlinear MSI regression equation shown in figure 9 fits the data for the 6-flight combination fairly well, with an r^2 of 0.929 and RMSE of 0.76°C ; however, the 2-band HSI data shown for the same flights in figure 7 is a much better fit, with an r^2 of 0.962 and RMSE of 0.55°C . When the 2002 data were added in to form the 9-flight combination, the fit for the MSI data, shown in figure 10, got much worse than the comparable 9-flight HSI data shown in figure 8. That the HSI data is much better than MSI for the larger range of conditions shows the need for careful selection of the filters for the MSI cameras. For the 9-flight combination, using 3-bands of MSI data, the resulting regression equation, in tables 8 and 9, showed that the coefficient for the green band was very small, and from

Table 8. Results of multiple linear regression on multispectral data.

Flight Combinations	MSI Bands	Linear Equations	r^2	RMSE (°C)
6 Flights	Green	$T_r = 9.14 - 96.01 * G$	0.139	2.65
	Red	$T_r = -7.05 + 294.6 * R$	0.476	2.07
	NIR	$T_r = 15.77 - 19.85 * N$	0.792	1.30
	Green, Red	$T_r = -1.61 - 94.70 * G + 293.5 * R$	0.612	1.78
	Green, NIR	$T_r = 13.49 + 106.5 * G - 26.06 * N$	0.886	0.97
	Red, NIR	$T_r = 8.15 + 148.2 * R - 16.19 * N$	0.886	0.97
	Green, Red, NIR	$T_r = 9.07 + 72.10 * G + 100.3 * R - 21.58 * N$	0.919	0.81
9 Flights	Green	$T_r = 7.90 - 76.17 * G$	0.181	2.37
	Red	$T_r = -4.34 + 211.0 * R$	0.340	2.13
	NIR	$T_r = 15.45 - 19.79 * N$	0.746	1.32
	Green, Red	$T_r = 0.55 - 84.86 * G + 224.4 * R$	0.563	1.73
	Green, NIR	$T_r = 15.01 + 33.15 * G - 22.43 * N$	0.767	1.26
	Red, NIR	$T_r = 9.49 + 124.8 * R - 17.30 * N$	0.854	1.00
	Green ^[a] , Red, NIR	$T_r = 9.60 + 6.24 * G + 121.0 * R - 17.87 * N$	0.854	1.00

[a] The contribution of G to this 3-parameter regression was not significant.

Table 9. Vegetation indices and results of nonlinear regression analysis on multispectral data, using the equation of the form $T_r = (c_1 - c_2 * I + c_3 * I^2) * e^{(I/c_4)}$.

Flight Combinations	MSI Bands	Vegetation Index (I)	c_1	c_2	c_3	c_4	r^2	RMSE (°C)
6 Flights	Green, Red ^[a]	$G - 3.099 * R$	0.40	20.32	588.6	10.0	0.629	1.74
	Green, NIR	$N - 4.086 * G$	13.24	45.19	38.57	0.52	0.892	0.94
	Red, NIR	$N - 9.151 * R$	8.37	25.25	19.09	1.70	0.899	0.91
	Green, Red, NIR	$N - 3.34 * G - 4.65 * R$	9.38	36.31	35.16	0.80	0.929	0.76
9 Flights	Green, Red ^[a]	$G - 2.644 * R$	1.22	15.46	987.2	10.0	0.636	1.58
	Green, NIR	$N - 1.478 * G$	19.77	50.11	31.83	2.00	0.786	1.21
	Red, NIR	$N - 7.213 * R$	10.55	29.56	20.69	3.00	0.877	0.92
	Green ^[b] , Red, NIR	$N - 0.349 * G - 6.768 * R$	10.67	31.38	23.27	2.20	0.878	0.91

[a] Minimum $T_r > 0$.

[b] The contribution of G to this 3-parameter regression was not significant.

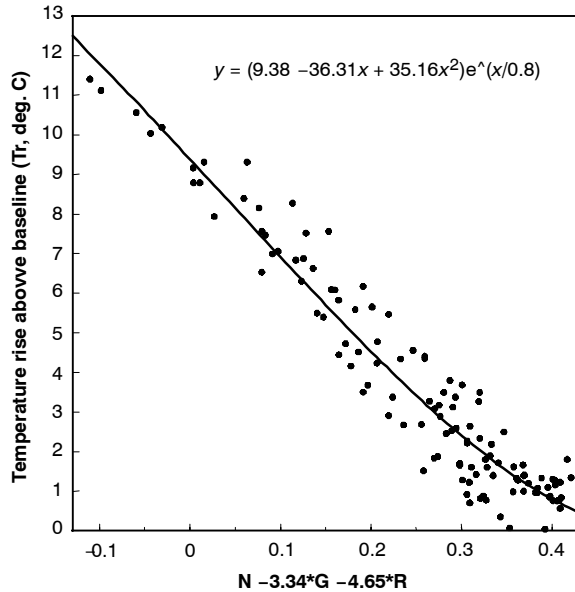


Figure 9. Rise in canopy temperature as a function of a 3-parameter MSI vegetation index for all data from 6 flights in 2001: $r^2 = 0.929$ and RMSE = 0.76°C .

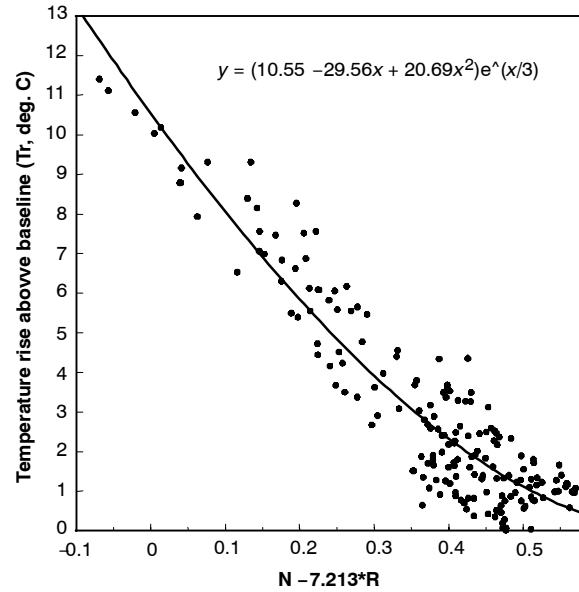


Figure 10. Rise in canopy temperature as a function of a 2-parameter MSI vegetation index for all data from 2001 and 2002 (9 flights): $r^2 = 0.877$ and RMSE = 0.92°C .

the regression analysis, adding green to the NIR and red combination did not significantly increase the r^2 value.

WEIGHTED NDVI

From the vegetation indices given in table 6, one notes that the coefficient on the visible (B35 to B60) term is always much greater than unity, and in all but one case the coefficient is between 8.8 and 11.1. These are very high weighting factors. Similarly, in table 9, when one of the terms in a 2-parameter vegetation index is NIR and the other is red, the coefficient on the red term is between 7.2 and 9.2 times that of the NIR term. This suggests a modification in the normalized difference vegetation index (NDVI) that puts equal weighting on the NIR and red terms. So, as seen in table 10, the vegetation indices from table 9 that contain only the NIR and red terms were normalized to the form $(N - w * R) / (N + w * R)$, where R is the reflectance from the red band, N is the reflectance from the NIR band, and w is the weighting factor. The correlation for the linear regression of this weighted NDVI is good for the combination of 6 flights from 2001, with an r^2 of 0.883, nearly the same as with the non-normalized regression results in table 8, which has an r^2 of 0.886.

Table 10. Results of simple linear regression of weighted NDVI as vegetation index.

No. of Flights	Vegetation Index (I) ^[a]	Linear Equation	r^2	RMSE (°C)
6	$\frac{N - 9.15 * R}{N + 9.15 * R}$	$T_r = 8.32 - 16.48 * I$	0.883	0.98
9	$\frac{N - 7.21 * R}{N + 7.21 * R}$	$T_r = 9.89 - 16.45 * I$	0.809	1.14

[a] N and R indicate the reflectances from the NIR and red bands.

Table 11. Results of nonlinear regression of weighted NDVI as vegetation index, using the equation of the form $T_r = (c_1 - c_2 * I + c_3 * I^2) * e^{(I/c_4)}$.

No. of Flights	c_1	c_2	c_3	c_4	r^2	RMSE (°C)
6	8.49	28.54	24.06	0.68	0.887	0.96
9	10.70	29.42	20.28	1.20	0.829	1.08

By comparing the results of the nonlinear regression analysis of the normalized indices in table 11 to the linear regression results in table 10, one can see that the correlation for the 6-flight data did not improve, suggesting that the basic data are linear. For the 9-flight data, there was some improvement in the r^2 value.

HIGH-DEFINITION STRESS IMAGE (HDSI)

The TIR image for the flight of 28 August 2001 for field 42 is shown in figure 11. From table 9, the best nonlinear regression equation for the 6-flight, 3-band, MSI data had an r^2 of 0.929, and it is shown here:

$$T_r = (9.381 - 36.31 \cdot I_{nrg} + 35.16 \cdot (I_{nrg})^2) \cdot e^{(I_{nrg}/0.8)} \quad (13)$$

where

$$I_{nrg} = N - 3.341 \cdot G - 4.646 \cdot R \quad (14)$$

G = reflectance from the green band.

Using Excel, columns representing equations 13 and 14 were added to the pixel-by-pixel data set for the flight date to form columns 6 and 7, respectively, as if they were additional bands. Columns 1 and 2 were the latitude and longitude of each pixel. T_r was then plotted as a function of the location coordinates using ArcView, and the result, the predicted temperature rise above the baseline, a measurement of stress, is shown in figure 12. The MSI image in figure 12 is much sharper than the TIR image in figure 11, one of the reasons being the difference in resolution, but with TIR there is also a certain amount of natural blurring of the temperatures, especially at the edges of the field. The 1.5 m wide access walkways are easily visible in figure 12 and not in figure 11. The entire field is stressed, but the B strip has less of a temperature rise than the rest of the field, and this effect stands out in both figures 11 and 12, but more clearly in the latter. We have named figure 12 a high-definition stress image (HDSI). The farm manager may appreciate being able to see the small hot spots before they become large hot spots. The relationship between the predicted temperature rise and the observed temperature rise is shown in figure 13. The r^2 is 0.898 and the RMSE is 0.72°C, which is 9.1% of the average temperature rise, all indicating a good prediction of plant water stress.

As far as how much of a temperature rise is too much, Reginato (1983) suggested that a temperature rise of 2°C to 3°C above the unstressed baseline for VPD values in the range of 2 to 4 kPa was optimum as a scheduling guide for irrigation of cotton, and according to Howell et al. (1984), it also corresponds to leaf water potentials of -1.7 to -1.8 MPa. There were still a few areas shown in figures 11 and 12 that had not passed this level, but most of the field was severely stressed.



Figure 11. TIR-based image for temperature rise for flight of 28 August 2001; 5-level quantile classification: white < 6.9°C < light gray < 8.5°C < gray < 10.47°C < dark gray < 14.58°C < black.

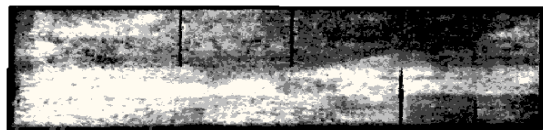


Figure 12. Temperature rise for flight of 28 August 2001 using MSI 3-parameter model; 5-level quantile classification: white < 6.42°C < light gray < 7.72°C < gray < 9.23°C < dark gray < 11.66°C < black.

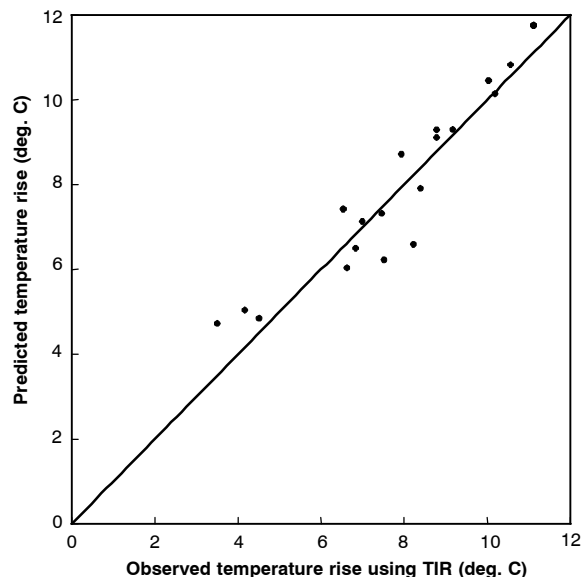


Figure 13. Temperature rise predicted by 3-parameter, 6-flight nonlinear MSI model compared to rise observed with TIR camera for 28 August 2001: RMSE = 0.72°C and r^2 = 0.898.

Table 12 shows the results of the validation tests. As one would expect, the performance of the validation sets was lower than for the calibration model. The RMSE is higher for the validation data set than for the calibration data set, but the difference would not be considered extreme. The ARPE values show an underprediction by 6.5% for the validation data set, primarily due to greater residuals at the higher temperatures ($T_r > 5^\circ\text{C}$). The r^2 values are very reasonable, and the EFF of 0.8 to 0.9 is exceptionally good. Negative values for EFF are classified as unacceptable, anything greater than zero can be called good, and anything above 0.5 is considered very high.

It was noticed in some cases that bands adjacent to the optimum band worked almost equally well as the optimum band. For example, in the 9-flight data of table 4, the first parameter of the 2-parameter HSI model could easily have been B16, B18, or B19, all which had nearly the same correlation as the optimum B17. In other cases, the adjacent bands were much less satisfactory, and the optimum bandwidth was very narrow. For example, no band other than B34 appears as the second term in the 9-flight data of table 4. Likewise for the 9-flight data in table 5, where no band other than B34 appears in the top 20 for the third term in a 3-parameter HSI model.

Goel et al. (2003), using essentially the same procedure as in this study, which is band selection with multiple regression, were successful in finding optimum bands for several biophysical properties of corn. They had only one 3-parameter model that had a higher r^2 than ours; it was 0.97 for plant greenness during one flight. Our best 9-flight, 3-parameter

Table 12. Validation with 2-band (B17, B34) model for 9 flights, using multiple linear regression on hyperspectral data.

Factor	Model Calibration	Validation
RMSE	0.617	0.851
EFF	0.937	0.894
ARPE	-0.0347	-0.065
r^2	0.931	0.907

linear HSI model had an r^2 of 0.940 and an RMSE of 0.63 °C, and the non-linear fit was even better. Goel et al. (2003) were concerned about the problem of collinearity or codependence of many band reflectances (Longley, 1967; Beaton et al., 1976) and suggested that with the goal of prediction rather than explanation, collinearity is less of a problem. Our study used a simple, straightforward multiple regression method for obtaining optimum bands, and it worked well over a wide range of field and atmospheric conditions. It resulted in a high degree of correlation between some new vegetation indices and field measurements. Especially significant is the weighted NDVI, which should require much less calibration than the normal NDVI. The results of this study can be used to better select the wavelengths used in the filters on the MSI cameras. With the proper filters on the MSI cameras, both the HSI camera and the TIR camera could be eliminated for detection of plant water stress, and there could be a very large reduction in the quantity of data that needs to be stored and manipulated.

CONCLUSIONS

This study shows that plant water stress can be measured with airborne MSI and HSI cameras flown over cotton fields. Very strong relationships were found between the rise in cotton canopy temperature above a baseline and several new vegetation indices under full-canopy conditions. The best 2-parameter indices are all of the form $T_r = N - w \cdot V$, where N is the reflectance from a band in the NIR range, V is the reflectance from a band in visible range, and w is a weighting factor that is much greater than unity. The w term is generally greater than 4, and is most often in the range of 7 to 11. The best combinations from the HSI data indicate which filters would be best fitted to the MSI cameras to get very sharp stress images. One of the best pairs of wavelengths found for all 9 flights combined was an NIR band of 686 nm and a visible band of 850 nm. The best fit for a 3-parameter model had bands centered at wavelengths of 686 nm, 811 nm, and 860 nm. For the 4-parameter model, the best fit was found with bands centered at 637 nm, 744 nm, 908 nm, and 1005 nm. One of the advantages of this procedure is that one can substitute HSI or MSI cameras for the TIR camera on board the plane. Differences in a broadband NIR values were found to be associated with differences in plant water stress. A good correlation was found between a weighted NDVI and plant water stress of Acala cotton.

REFERENCES

Allen, R. G., L. S. Pereira, D. Raes, and M. Smith. 1998. Crop evapotranspiration guidelines for computing crop water requirements. Irrigation and Drainage Paper No. 56. Rome, Italy: Food and Agriculture Organization of the United Nations.

Beaton, A. E., D. B. Rubin, and J. L. Barone. 1976. The acceptability of regression solutions: Another look at computational accuracy. *J. American Stat. Assoc.* 71(353): 158-168.

Bowman, W. D. 1989. The relationship between leaf water status, gas exchange, and spectral reflectance in cotton leaves. *Remote Sensing Environ.* 30(3): 249-255.

Dawson, C. J. 1997. Management of spatial variability. In *Precision Agriculture '97, Vol. I: Spatial Variability in Soil and Crop*, 45-58. J. V. Stafford, ed. Oxford, U.K.: BIOS Scientific Publishers.

DeTar, W. R. 2004. Using a subsurface drip irrigation system to measure crop water use. *Irrigation Sci.* 23(3): 111-122.

Ehrler, W. L., S. B. Idso, R. D. Jackson, and R. J. Reginato. 1978. Wheat canopy temperature: Relation to plant water potential. *Agron. J.* 70(2): 251-256.

Goel, P. K., S. O. Prasher, J. A. Landry, R. M. Patel, A. A. Viau, and J. R. Miller. 2003. Estimation of crop biophysical parameters through airborne and field hyperspectral remote sensing. *Trans. ASAE* 46(4): 1235-1246.

Howell, T. A., J. L. Hatfield, H. Yamada, and K. R. Davis. 1984. Evaluation of cotton canopy temperature to detect crop water stress. *Trans. ASAE* 27(1): 84-88.

Idso, S. B., R. J. Reginato, and S. M. Farah. 1982. Soil and atmosphere induced plant water stress as inferred from foliage temperatures. *Water Resources Res.* 18(4): 1143-1148.

Jackson, R. D., S. B. Idso, R. J. Reginato, and P. J. Pinter, Jr. 1981. Canopy temperature as a crop stress indicator. *Water Resources Res.* 17(4): 1133-1138.

Jackson, R. D., P. N. Slater, and P. J. Pinter, Jr. 1983. Discrimination of growth and water stress in wheat by various vegetation indices through clear and turbid atmospheres. *Remote Sensing Environ.* 13(3): 187-208.

Jakeman, A. J., I. G. Littlewood, and P. G. Whitehead. 1990. Computation of the instantaneous unit hydrograph and identifiable component flows with application to two small upland catchments. *J. Hydrology* 117: 275-300.

Legates, D. R., and G. J. McCabe, Jr. 1999. Evaluating the use of "goodness-of-fit" measures in hydrologic and hydroclimatic model validation. *Water Resources Res.* 35(1): 233-241.

Longley, J. W. 1967. An appraisal of least squares procedures for electronic computer from the point of view of the user. *J. American Stat. Assoc.* 62(319): 819-841.

Maas, S. J. 1998. Estimating cotton canopy ground cover from remotely sensed scene reflectance. *Agron. J.* 90(3): 384-388.

Maas, S. J., G. J. Fitzgerald, W. R. DeTar, and P. J. Pinter, Jr. 1999. Detection of water stress in cotton using multispectral remote sensing. In *Proc., Beltwide Cotton Conf.*, 2: 584-585. Memphis, Tenn.: National Cotton Council.

Moran, M. S., P. J. Pinter, Jr., B. E. Clothier, and S. G. Allen. 1989. Effect of water stress on the canopy architecture and spectral indices of irrigated alfalfa. *Remote Sensing Environ.* 29(3): 251-261.

Moran, M. S., Y. Inoue, and E. M. Barnes. 1997. Opportunities and limitations for image-based remote sensing in precision crop management. *Remote Sensing Environ.* 61(3): 319-346.

Nash, J. E., and J. V. Sutcliffe. 1970. River flow forecasting through conceptual models: Part I. A discussion of principles. *J. Hydrology* 10(3): 282-290.

Peñuelas, J., I. Filella, L. Serrano, and R. Savé. 1996. Cell wall elasticity and water index (R970 nm /R900 nm) in wheat under different nitrogen availabilities. *Int. J. Remote Sens.* 17(2): 373-382.

Pinter, P. J., Jr., and R. J. Reginato. 1982. A thermal infrared technique for monitoring cotton water stress and scheduling irrigations. *Trans. ASAE* 25(6): 1651-1655.

Plant, R. E., D. S. Munk, B. R. Roberts, R. L. Vargas, D. W. Rains, R. L. Travis, and R. B. Hutmacher. 2000. Relationships between remotely sensed reflectance data and cotton growth and yield. *Trans. ASAE* 43(3): 535-546.

Reginato, R. J. 1983. Field quantification of crop water stress. *Trans. ASAE* 26(3): 772-775, 781.

Thenkabail, P. S., R. B. Smith, and E. DePauw. 2000. Hyperspectral vegetation indices and their relationships with agricultural crop characteristics. *Remote Sensing Environ.* 71(2): 158-182.

Thorp, K. R., L. Tian, H. Yao, and L. Tang. 2004. Narrow-band and derivative-based vegetation indices for hyperspectral data. *Trans. ASAE* 47(1): 291-299.

Wanjura, D. F., and D. R. Upchurch. 2000. Canopy temperature characterizations of corn and cotton water status. *Trans. ASAE* 43(4): 867-875.

